Electronic Structure of a Transient Histidine Radical in Liquid Aqueous Solution: EPR Continuous-Flow Studies and Density Functional Calculations

Günter Lassmann,*,† Leif A. Eriksson,‡ Fahmi Himo,§ Friedhelm Lendzian,† and Wolfgang Lubitz†

Max-Volmer-Institut fur Biophysikalische Chemie und Biochemie, Technische Universität Berlin, D-10623 Berlin, Germany, Department of Quantum Chemistry, Uppsala University, Box 518, S-75120 Uppsala, Sweden, and Department of Physics, Box 6730, Stockholm University, S-11385 Stockholm, Sweden

Received: November 3, 1998

Transient histidine radicals formed in aqueous solutions by oxidation of histidine with a Ti^{3+}/H_2O_2 Fenton system at pH 2.0 have been studied by EPR using a fast continuous-flow setup and a dielectric ring resonator equipped with a mixing chamber. A histidine peroxy radical with a single EPR line at $g = 2.0151$ and a histidine cation radical with a complex hyperfine structure and $g = 2.0023$ have been detected. The hyperfine structure of the latter radical was analyzed by investigating two selectively deuterated histidines and using an EPR simulation and fit program for analysis of the spectra. Isotropic hyperfine coupling constants of two β-protons, three ring protons, and two nitrogen nuclei have been determined in this way and assigned to a histidine−OH adduct cation radical. Density functional theory (DFT) calculations at the B3LYP and PWP86 levels have been performed on protonated cation radicals of 4-ethylimidazole (as histidine models), yielding isotropic hyperfine coupling constants for three different positions of OH addition. The C5 position for OH addition (a 5-oxohistidine cation radical) is clearly supported by the calculated hyperfine coupling constants. The agreement between DFT and EPR is further improved when hydrogen-bonding interactions to the N1 and C2 protons are introduced in the calculations.

1. Introduction

In many metal enzymes histidine is a ligand of a metal ion in the active site and influences the redox properties of these complexes. Radical enzymes exhibiting radicals of certain amino acid side chains, which are essential for the catalytic function, also frequently contain redox-active metal complexes as a part of the functional electron/radical transfer pathway. Catalytically essential amino acid radicals in radical enzymes have been observed from tyrosine in ribonucleotide reductase (RR),[1,2] prostaglandin H synthase,[3] photosystem II,[4] and galactose oxidase,[5] from tryptophan in DNA photolyase[6] and cytochrome *c* peroxidase,[7] and from glycine in pyruvate formate lyase[8] and anaerobic RR.[9] A transient cysteine radical has been postulated for the catalytic turnover in RR.[10,11] It is reasonable to assume that transient histidine radicals may also occur as metal ligands in the electron or radical transfer pathways of radical enzymes.[11] More generally, transient histidine ligand radicals may play a role during redox reactions of metalloproteins.

In Ca-depleted samples of the oxygen-evolving photosystem II complex, radicals from an oxidized histidine have been postulated from an optical absorption band at 310 nm (similar to that observed from a histidine OH-adduct radical[12]) and a broad unstructured EPR line which has been simulated as a species with a weak spin-exchange between a radical and a metal site.[13,14] Although ESEEM studies have suggested histidines as ligands for the Mn cluster in photosystem II[14,15] data on hyperfine coupling constants of this postulated histidine radical are still missing. Meanwhile, a tyrosine-based radical is discussed alternatively in this system.[16]

Nevertheless, there is no direct EPR spectroscopic evidence for a protein-linked histidine radical as reported for tyrosine radicals in R2 protein of RR[2,11] and tryptophan radicals in mutants of R2 proteins.[17,18] This could have several reasons. (i) One main reason may be the higher redox potential of histidine (1.4 V) in comparison with tyrosine (0.85 V) and tryptophan (0.90 V; measured in amino acids at pH 4.0 with electrooxidation using a graphite electrode[19]). (ii) The lifetime of a protein-linked radical depends strongly on the protein environment; it can be long-lived if it is buried in a hydrophobic pocket and shielded from the external aqueous medium, e.g. $Tyr^{\bullet}$ in RR,[2] or very short-lived if it is exposed to the medium, e.g. $Trp^{\bullet}$ in DNA photolyase.[6] In the latter case, detection by EPR would be difficult. (iii) Another difficulty in EPR studies of protein radicals arises from the oftenly observed magnetic interaction with paramagnetic metal centers, which in many radical enzymes are close to the radical site. In such a case, spin exchange leads to a strong increase of relaxation rates of the radical and EPR can be detected only at low temperatures. An example is $Trp^{\bullet}$ in cytochrome *c* peroxidase.[7] These difficulties, in particular the close proximity of a possible histidine radical to a ligating paramagnetic metal, may probably be the reason that so far protein-linked histidine radicals have not been observed and analyzed by EPR. An example for a strong magnetic interaction between a metal site and a radical from an amino acid ligand is found in galactose oxidase. Here a tyrosine radical ($S = {}^1/_2$) is ligated to a paramagnetic Cu^{2+} ($S = {}^1/_2$) (distance: 2 Å) which, in this case, leads to an antiferromagnetic spin coupling and an EPR silent ground state.[5]

* To whom correspondence should be addressed.
† Technical University of Berlin.
‡ University of Uppsala.
§ University of Stockholm.

10.1021/jp9843454 CCC: $18.00
Published on Web 02/13/1999

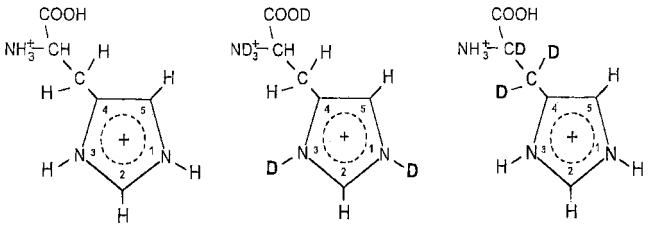

Figure 1. Histidine derivatives as used for generation of radicals by Fenton oxidation in aqueous solution at pH 2, with numbering scheme of ring positions; A, histidine in H_2O, fully protonated; B, histidine in D_2O, deuterated at dissociable proton positions; C, α,β,β-deuterated histidine (in H_2O).

From histidine being not involved in a polypeptide chain, EPR and ENDOR data on different types of histidine radicals have been reported earlier. In single crystals of histidine hydrochloride X-irradiated at low temperature, primary radicals were observed upon decarboxylation and H-atom addition to the carbonyl oxygen or by one-electron oxidation yielding a histidine cation radical on the imidazole ring.[20] The hyperfine coupling tensors for two ring α-protons of the cation radical (isotropic values: 1.06 and 1.21 mT) have been determined, but no hyperfine data were given for β-protons and imidazole nitrogens. A stable secondary histidine radical in histidine hydrochloride crystals irradiated at room temperature was formed by hydrogen addition to the imidazole ring resulting in two large proton couplings (isotropic value: 4.7 and 5.0 mT).[21] A deamination radical and carboxyl anion radicals have also been observed in X-irradiated single crystals of histidine dihydrochloride.[22]

EPR and ENDOR data of X-irradiated single crystals of imidazole were published for a radical which is formed in a reducing step upon H-addition to the C2 position (for C-numbering of the imidazole ring, see Figure 1). Hyperfine (hf) tensors for all α-protons were determined, but no data for nitrogens were submitted. Experimentally derived spin densities at the ring atoms of imidazole were compared with those obtained by Hückel, McLachlan, and INDO calculations.[23]

Radicals from imidazole in the liquid state formed upon reaction at pH 9−10 with hydroxyl radicals by steady-state *in-situ* radiolysis[24] or by a Fenton reaction at pH 2 in a steady-state flow-system[25] have been studied by EPR. In both cases, OH addition at the C5 position leads to the imidazole radical, and isotropic hyperfine coupling constants for α-protons and nitrogens were determined. The kinetics of formation and decay of cation radicals from imidazole and histidine formed after reaction with OH radicals under radiolysis conditions were studied by optical spectroscopy monitoring the 310 nm absorption peak.[12] For histidine radicals formed by oxidation, however, a comparable set of hf data in the liquid state including β-protons does not exist. Therefore, EPR studies on histidine radicals in model systems are necessary in order to elucidate typical spectral features of such radicals in order to recognize them more easily in different proteins.

In electron transfer reactions during enzyme catalysis, histidine radicals with the unpaired electron localized on the imidazole ring are expected upon one-electron oxidation. In the case of protein damage, however, upon oxidative stress, e.g. by an attack on the protein by active oxygen species (hydroxyl radicals, superoxide radicals, or singlet oxygen), or upon radiation damage (UV light or X-irradiation), OH radicals may attack the imidazole ring leading to histidine−OH adduct radicals. Previously, formation of histidine radicals was reported as a result of H-atom addition and deamination only, and there are little data on species created by oxidation.

The aim of the present paper is to identify the radical formed by oxidation of histidine in aqueous medium and determine the isotropic hyperfine coupling constants and spin density distribution from highly resolved EPR spectra. A comparison with density functional theory (DFT) calculations of isotropic hyperfine coupling constants and spin density at the ring atoms for radicals of the histidine model 4-ethylimidazole with OH addition at three different position is presented.

This is the first report on a detailed electronic structure, including hyperfine couplings of β-protons, ring protons, and nitrogens, of a histidine radical in aqueous solution determined by EPR spectroscopy and confirmed by density functional calculations.

2. Materials and Methods

2.1. Generation of Radicals. A Ti^{3+} Fenton system at pH 2.0 [26−28] was used in order to generate histidine radicals by oxidation of histidine by OH radicals according to the following reaction sequence:

$$Ti^{3+} + H_2O_2 \rightarrow {}^{\bullet}OH + OH^- + Ti^{4+}$$
$$^{\bullet}OH + His \rightarrow HisOH^{\bullet} \qquad (1)$$

The two solutions which were mixed in the continuous-flow system at pH 2.0 contained the following components. Reactant I: histidine (10, 40, and 80 mM, respectively); H_2O_2 (500 mM); pH 2.0; Reactant II: histidine (10, 40, and 80 mM, respectively); $TiCl_3$ (14 mM).

L-Histidine was obtained from Bachem; $TiCl_3$ and H_2O_2 from Fluka. D_2SO_4, NaOD, and D_2O were bought from Sigma; DL-α,β,β-d_3-histidine was from CDN Isotopes, Quebec, Canada.

Generation of histidine radicals in D_2O was performed using D_2SO_4 and NaOD for pH adjustment. The given concentration of H_2O_2 diluted in D_2O contributes only 2.5% H in the assay.

2.2. Continuous-Flow EPR Setup. A Bruker ESP 300E EPR spectrometer was used in combination with the dielectric mixing resonator ER 4117 D-MVT. This accessory combines a two-component mixer with a dielectric ring X-band resonator and allows continuous-flow EPR studies with low consumption of reactants. The EPR cell is a thick-walled quartz capillary of 0.4 mm i.d. surrounded by a sapphire ring. This setup has a high sensitivity for a small volume (2 μL) of aqueous samples. The cross-section of the EPR tube is 11 times less than the 5-mm quartz flat cell and 16 times less than the 10-mm flat cell. Considering the same linear flow rate, e.g. the same time resolution, the volume flow rate in this mixing resonator which determines the consumption of reactants is less by a factor 11 and 16, respectively, than in the corresponding conventional EPR X-band mixing devices mentioned above. This advantage allows the use of expensive isotopically substituted substances (see Figure 3C) with acceptable consumption of reactants. The reactants I and II in the two 30 mL syringes (polypropylene) to be mixed are driven simultaneously by a syringe pump (Harvard 22, Kleinfeld Laboratories, Hannover, Germany) via connecting tubes (0.6 mm i.d. PEEK) through the mixer and the EPR sample tube. The speed of the stepping motor of the pump is programmable and microchip-controlled.

A volume flow rate of 34 mL/min (corresponding to a linear flow rate of 4.4 m/s) was used for generation of the histidine radicals. The dead-time between the mixer cell and the EPR-active volume at the fastest flow used is 1 ms, but a sufficiently high steady-state concentration of these short-lived histidine

radicals is achieved probably because of the intentional incomplete mixing efficiency of the Y-mixer so that mixing takes place mainly within the EPR cell rather than in the mixer. With a flow rate of 34 mL/min two accumulated 20 s scans consumed about 150 mg of $\beta\beta$-deuterated histidine (40 mM in both of the two syringes) in order to acquire the EPR spectrum shown in Figure 3C.

Fremy's salt (potassium peroxylamine disulfonate) with $g = 2.0055 \pm 0.0001$ was used as an appropriate *g*-factor standard for the flow resonator.

2.3. Analysis of Spectra. The simulation of isotropic EPR spectra was performed on a HP work station using a simulation program for EPR described in ref 17. This program allows a nonlinear least-squares fit routine to find the optimum set of parameters for the best simulation of a given experimental EPR spectrum.[29]

2.4. Density Functional Theory Calculations. Complementary to the experimental study, detailed theoretical analyses were conducted on a number of hydroxylated imidazole radicals, as described below. By comparing theoretical and experimental hyperfine coupling constants, it is possible to select the type of radical fitting optimally to the experimentally observed radical. Theoretical studies of radical hyperfine properties, although conducted at various levels during some 30 years, have recently witnessed a tremendous breakthrough with the development and implementation of so-called gradient-corrected density functional theory (DFT) or hybrid Hartree−Fock (HF)−DFT approaches.[30] Due to a more favorable scaling with increasing size of the system compared with conventional accurate *ab initio* based methods, it is possible with the DFT-based approaches to investigate systems of far larger size than previously possible, while still retaining accuracy.

Through detailed investigations and comparisons between various DFT functionals, two have been singled out as being by far the most accurate for hyperfine properties, B3LYP and PWP86.[31] The former is based on a combination of HF exchange and gradient-corrected DFT exchange and correlation (Slater local and Becke's 1988 gradient corrected exchange; Vosko−Wilk−Nusair local and Lee−Yang−Parr gradient corrected correlation).[32] Their relative contributions were determined from a least-squares fit to atomization energies, ionization potentials, and electron affinities of a large number of systems. PWP86, on the other hand, is a "pure" DFT functional, using the gradient correction to the exchange by Perdew and Wang and to correlation by Perdew.[33] In the present paper, all systems investigated were optimized at the B3LYP/6-31G(d,p) level, using the Gaussian 94 program.[34] These were followed by single point PWP86/6-311G(2d,p) calculations using the deMon code,[35] in order to evaluate the hyperfine coupling constants for the systems. This particular combination of approaches has recently been employed in several studies of radicals of biophysical interest[36−38] and proven to yield highly accurate results.

The systems investigated are cation radicals from 4-ethylimidazole at low pH (both nitrogens protonated) hydroxylated at three different positions as models of the experimentally investigated hydroxylated histidine cation radicals at pH 2. For all systems we report atomic spin densities and isotropic hyperfine couplings; we have also investigated effects of hydrogen bonding.

3. Results and Discussion

3.1. Identification of Radicals upon Fenton Oxidation of Histidine. The histidine radicals have been generated in a Ti^{3+} Fenton reaction at pH 2.0 using a flow system (as described above). Without any substrate (histidine), the OH radicals generated in the Fenton system form transient Ti^{4+}−peroxy complexes showing an unresolved single EPR line (line width $\Delta H = 0.12$ mT) with $g = 2.0135$, a *g*-factor typical for peroxide radicals as observed earlier[39,40] (Figure 2A). At histidine concentrations between 5 and 20 mM another single EPR line ($\Delta H = 0.17$ mT) appears at $g = 2.0151$ (Figure 2B), which is absent without the substrate histidine (Figure 2A). The amplitude of this line increases with increasing concentration of histidine from 5 to 20 mM. Above 20 mM histidine it decreases and a complex EPR spectrum is formed with an isotropic *g*-factor of 2.0023 (Figure 2C). Up to 80 mM histidine, the intensity of the complex EPR spectrum increases with a concomitant decrease of the intensity of the EPR line at $g = 2.0151$. Since both signals exist only in presence of histidine and depend on its concentration, they are regarded as belonging to histidine-derived radicals. Both are short-lived on a submillisecond time scale because their intensities increase with faster flow rates (up to 34 mL/min).

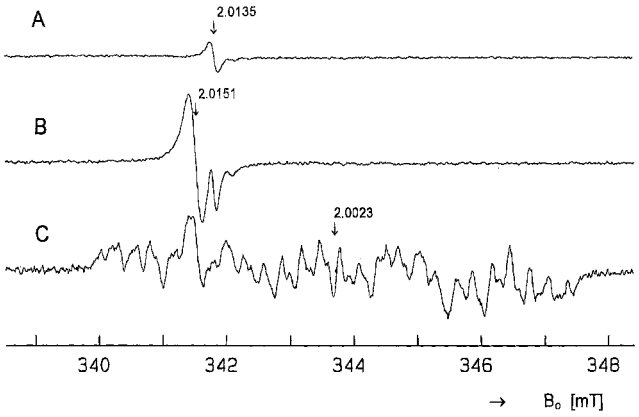

Figure 2. EPR continuous-flow spectra of histidine after reaction with OH radicals in a Ti^{3+}/H_2O_2 Fenton system at pH 2.0 with various concentrations of histidine. Experimental conditions: microwave power, 3 mW; modulation, 100 kHz/0.05 mT); sweep time, 20 s (A, C), 40 s (B); time constant, 20 ms (A, C), 40 ms (B); 1 scan (A, B), 2 scans (C); flow rate, 34 mL/min. A: no histidine (control); reactant I, [H_2O_2] 500 mM; reactant II, [Ti^{3+}] 14 mM. B: reactant I, [H_2O_2] 500 mM, [His] 10 mM; reactant II, [Ti^{3+}] 14 mM, [His] 10 mM. C: reactant I, [H_2O_2] 500 mM, [His] 40 mM; reactant II, [Ti^{3+}] 14 mM, [His] 40 mM.

The Ti^{4+}−peroxy complex competes for the OH radicals with the substrate histidine and disappears with higher concentrations of histidine (Figure 2C). A hyperfine structure from ^{47}Ti and ^{49}Ti isotopes as seen earlier on an intense line of the Ti^{4+}−peroxy complex[39,40] was not observed on the histidine-derived line at $g = 2.0151$. From the close similarity of the *g*-factor of the histidine single line to those of the peroxytitanium complex and to known organic peroxy radicals[41] as well as from the narrow line width and the absence of hf splitting, we assume that the single line at $g = 2.0151$ belongs to a histidine peroxy radical (his−O−O•) with spin density localized mainly at the two oxygens.[42] This is in accordance with the observation that the histidine peroxy radical dominates at higher concentrations of H_2O_2.

At higher concentrations of histidine, however, the preferred reaction of OH is the formation of the histidine radical which exhibits the complex EPR spectrum (Figure 2C). The large number of lines suggests that the unpaired spin is localized mainly in the imidazole ring of histidine and interacts with several nuclei (Figure 1A). This histidine radical is the subject of a detailed analysis of its hyperfine structure, as outlined

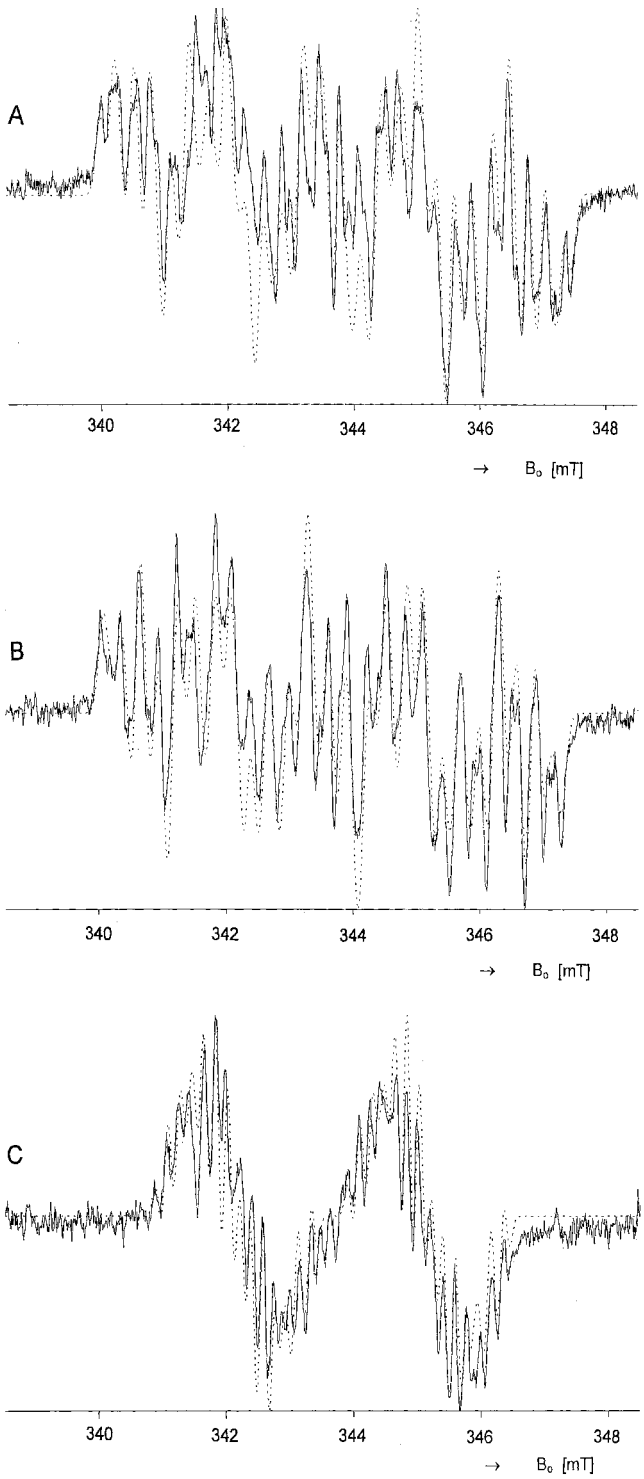

Figure 3. EPR spectra of transient histidine radicals formed by oxidation in a Ti^{3+}/H_2O_2 Fenton system at pH 2.0, recorded by continuous flow. The single line occurring at 341.5 mT (see Figure 2B) has been subtracted prior to the simulation and fit procedure. (Dotted line: best simulation using the hfc's given in Table 1.) Experimental conditions: microwave power, 3 mW; modulation, 100 kHz/0.05 mT; time constant, 20 ms. A: histidine in H_2O; reactant I, $[H_2O_2]$ 500 mM, [His] 80 mM; reactant II, $[Ti^{3+}]$ 14 mM, [His] 80 mM; flow rate, 38 mL/min; sweep time, 40 s; 5 scans. B: histidine in D_2O; reactant I, $[H_2O_2]$ 500 mM, [His] 80 mM; reactant II, $[Ti^{3+}]$ 14 mM, [His] 80 mM; flow rate, 34 mL/min; sweep time, 20 s; 3 scans. C: α,β,β-d_3-histidine in H_2O; reactant I, $[H_2O_2]$ 500 mM, [His] 40 mM; reactant II, $[Ti^{3+}]$ 14 mM, [His] 40 mM; flow rate, 34 mL/min; sweep time, 20 s; 2 scans.

below. Since this EPR spectrum extends over 7.4 mT, the amplitude of the first derivative is, at the same concentration, about 3 orders of magnitude smaller than for the narrow single line of the proposed histidine peroxy radical at $g = 2.0151$. The steady-state concentration of the transient histidine radical depends on its lifetime, the geometry of the mixer and the EPR cell, the flow rate, and on the concentrations of the reactants. Since the amplitude of the EPR signal is maximal at fastest flow rate and collapses immediately after stopping the flow, the lifetime of the radical is probably shorter than 1 ms.

In order to obtain EPR spectra of sufficient intensity and resolution, it was necessary to perform a detailed optimization of the concentration of the reactants. Optimal conditions for sufficient concentration of histidine radicals are found for concentrations $[H_2O_2] \gg [S] > [Ti^{3+}]$ with the used Fenton system which is in agreement with those reported for other organic compounds[25−27] too (S: substrate to be oxidized in the Fenton system, here histidine). The results of this procedure, e.g. the optimal concentrations of all reactants, are given in the legend of Figure 3.

3.2. Structure of a Histidine OH-Adduct (Cation) Radical in Liquid Aqueous Solution. *3.2.1. Hyperfine Structure Analysis of the Isotropic EPR Spectra.* For unraveling the complex EPR hyperfine spectrum of histidine radicals, two selectively deuterated histidines have been used in addition to the normal histidine: (i) All dissociable NH and OH protons were replaced by dissolving histidine in D_2O (Figure 1B). (ii) Histidine with deuterated β-protons (dissolved in H_2O) was used (Figure 1C). The EPR spectra at pH 2 from Fenton-oxidized histidine in H_2O, histidine in D_2O, and $\beta\beta$-deuterated histidine (in H_2O) are shown in Figure 3A−C, respectively. The single EPR line at $g = 2.0151$ (from a histidine peroxy radical; see also Figure 2B,C) has been subtracted in all three spectra shown in Figure 3. Although the relative concentration of the species from the single EPR signal is less than 2% of the concentration of the multiline pattern, this approach was necessary for the fitting process in the spectral simulations.

Considering the large splittings, the spectral analysis shows five spectral groups with an integral intensity of about 1:2:2:2:1 for both histidine in H_2O as well as in D_2O (Figure 3A,B) which corresponds to one large proton splitting of about 3.0 mT and two nearly equivalent proton splittings of about 1.5 mT. All these protons are nondissociable. Histidine radicals with deuterated β-protons show only the large proton splitting and lack the other two (Figure 3C). This indicates that the two, nearly equivalent proton splittings in the unmodified histidine sample belong to the two β-protons of the histidine radical.

The smallest hyperfine couplings are best visible in the wings of the spectrum for histidine in D_2O (Figure 3B) and correspond to two nitrogen nuclei ($I = 1$) with different splittings (0.14 and 0.27 mT). For histidine in H_2O an additional small doublet splitting (0.18−0.20 mT) from an exchangeable proton ($I = {}^1/_2$) is additionally involved. Accordingly, this proton-splitting is missing in the total width of the D_2O−histidine spectrum (7.16 mT) as compared to that of histidine in H_2O (7.33 mT) (see Table 1). It turned out in the spectral simulations that a further proton splitting of 0.58 mT was required in addition. The most complicated spectrum, of β-deuterated histidine in H_2O, was fitted using the data set of histidine in H_2O and by replacing the two β-proton coupling by the correspondingly smaller (resolved) deuteron splittings (see Figure 3C and Table 1). The smaller total width of the spectrum (5.48 mT) for the *ββ-deuterated* histidine radical corresponds to the larger value (7.33 mT) from the *ββ-protonated* radical and is nicely reproduced by the simulation which further supports the given assignment.

TABLE 1: Isotropic Hyperfine Coupling Constants (mT) of the Histidine−OH Adduct Cation Radical Derived from EPR Experiments and Used for Spectra Simulation (Error: ±0.02 mT)

molecular posn	His in H_2O[a] (fully protonated)	His in D_2O (NH-deuterated)	α,β,β-deuterated His[a] (in H_2O)
a(H5)	3.02	3.02	3.02
a(Hβ1)	1.41	1.41	0.22[b]
a(Hβ2)	1.23	1.23	0.19[b]
a(H2)	0.58	0.59	0.59
a(H_{NH} or H_{OH})	0.21	<0.03	0.21
a(N1)	0.14	0.14	0.14
a(N3)	0.27	0.27	0.28
line width[c]	0.08	0.09	0.06
tot. width[d]	7.33	7.16	5.48

[a] Corresponding formulas in Figure 1. [b] Deuteron coupling constants. [c] Width of individual lines used for simulation. [d] Between turning points of outermost EPR lines in spectra of Figure 3.

The complete set of hyperfine coupling constants obtained from the best least-squares fit of the spectra (dotted lines in Figure 3) are listed in Table 1 for the three different histidine radicals. The hfc's of two nitrogens and five protons in the case of histidine in H_2O (Figure 1A) are in excellent agreement with those of the corresponding radical of histidine in D_2O (two N's, four H's; Figure 1B) and those of β-deuterated histidine in H_2O (two N's, two D's, three H's; Figure 1C).

3.2.2. Assignment of Hyperfine Splittings to Protons and Nitrogens of the Histidine Radical. The two isotropic splittings of 1.41 and 1.23 mT in the EPR spectrum of normal histidine in H_2O, which reduce to 0.22 and 0.19 mT in case of β-deuterated histidine, belong without any doubt to the two β-protons. A large isotropic proton splitting of 2.64 mT was previously observed by EPR in the liquid state after $OH^•$ attack on imidazole upon *in-situ* pulse radiolysis at pH 9−10.[24] In the case of oxidation of imidazole using the same Ti^{3+}/H_2O_2 Fenton system at pH 2.0 as employed here, and a similar EPR continuous-flow device in Q-band, a large proton splitting of 3.03 mT—very close to our value (3.02 mT)—has been observed.[25] In both cases, this large splitting has been assigned to a ring proton (bent out-of-ring plane) linked to the tetragonal C5 ring carbon atom in the imidazole radical formed after addition of an OH radical to that carbon which originally was trigonal. Thus, the α-proton on C5 is in a β-position with respect to C4 where the maximum spin density resides (see below). Large isotropic hfc's up to 4.0 mT have also been reported from ring protons after H-atom addition, in X-irradiated histidine single crystals.[21,23] Thus, we interpret the large proton splitting in the present sample as originating from a CH proton of the imidazole ring after addition of an OH radical to the C5 (or C2) carbon (for the position of the OH addition, see also section 3.2.3). Taking this into account, the type of observed histidine radical upon Fenton oxidation is an OH-adduct radical. According to the pK = 6.5 of histidine and pK = 5.5 of the corresponding OH-adduct radical,[12] the protonation of both imidazole nitrogens of histidine at pH 2.0 suggests that after addition of a neutral OH radical from the Fenton system to the positively charged histidine we observe a histidine *cation* radical.

The proton splitting of 0.58 mT which appears in all three histidine EPR spectra (Table 1) belongs to the α-proton on the C2 (or C5) ring carbon which is *not* attacked by $OH^•$. In the similar imidazole cation radical at pH 2.0 a corresponding α-proton splitting of 0.66 mT was observed,[25] which is close to our value. In the neutral imidazole radical at pH 9−10, a larger value (0.99 mT) was found for the C2 α-proton.[24]

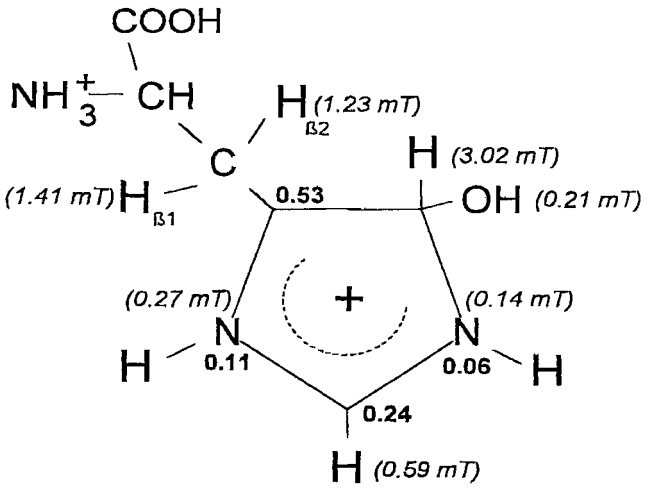

Figure 4. Electronic structure (hyperfine coupling constants and π-spin densities) determined *experimentally* by EPR spectroscopy for the histidine−OH adduct cation radical at pH 2.0. Isotropic hyperfine coupling constants (in brackets and italic letters) are given next to the corresponding nuclei; the respective π-spin densities are given in bold letters.

The position of the exchangeable proton with a splitting of 0.21 mT of the histidine cation radical is still open. It may belong to one of the two ring NH protons or to the OH proton at the OH adduct. DFT data for the 4-ethylimidazole cation radical with C5−OH addition favor the OH proton (0.22 mT) or the N1−H proton (0.29 mT) but not the N3−H proton (0.005 mT) (Figure 5D). It is not yet clear why the second exchangeable proton, which according to the calculations should have a resolvable splitting, is not visible in the EPR spectra.

Both nitrogen hyperfine coupling constants (0.14 and 0.27 mT) have been resolved in the EPR spectrum of the OH-adduct histidine cation radical (see Table 1). The assignment of the smaller value to N1 and the larger to N3 in the histidine cation radical is based on DFT calculations (see section 3.2.3). Figure 4 summarizes the assignment of the *experimentally* observed hfc's to the individual nuclei of the histidine radical (in italic letters). These hfc's are directly correlated with the distribution of the spin density in the radical. This experimentally established electronic structure of a histidine cation radical forms the basis for a comparisons with calculated hyperfine data, in order to test advanced quantum chemical methods.

Spin Densities Derived from Isotropic EPR Hyperfine Coupling Constants. For α-protons of an aromatic ring the π-spin density ρ_C at the connecting C-atom can be estimated from the isotropic proton coupling constant $a^{\alpha}{}_H$ using the McConnell relation $a^{\alpha}{}_H = \rho_C Q$, with Q = 2.48 mT.[43,44] Following this empirical relation a π-spin density at C2 of ρ(C2) = 0.24 is derived from the C2 α-proton. The isotropic β-proton coupling constant $a^{\beta 1,2}{}_H$ is related via a hyperconjugation mechanism to the π-spin density ρ_C at the neighboring C-atom according to $a^{\beta 1,2}{}_H = \rho_C Q' \cos^2 \theta_{1,2}$, with Q' = 5.0 mT [43] and the dihedral angles $\theta_{1,2}$ between the projection of the C−H$^{\beta}$ bond and the direction of the p_z-orbital perpendicular to the ring plane. Assuming rapid rotational fluctuations (waggling) of the methylene group of the histidine radical in liquid solution at room temperature about the C4−C$_{\beta}$ bond, the θ angles of the two β-protons are averaged out to a certain extent and $\cos^2 \theta_{1,2}$ attains the mean value $^1/_2$. Thus, $a^{\beta 1}{}_H \approx a^{\beta 2}{}_H = \rho_{C4} Q'^1/_2$, with the mean value of the two β-hfc's (1.32 mT) yielding ρ(C4) = 0.53. The small but significant inequivalence of $a^{\beta 1}{}_H$ and $a^{\beta 2}{}_H$

can be explained by the asymmetry near the methylene group. Particularly, the chiral carbon center adjacent to the methylene group occurring in all amino acids has been shown to be responsible for the inequivalence of the two methylene β-protons in case of a tyrosyl radical in liquid aqueous systems.[45] This situation seems to be quite similar also in case of the histidine radical as observed here.

The π-spin density at the nitrogens can be estimated using the corresponding formula $a^N = \rho^{\pi}_N Q^N$ with $Q^N = 2.5$ mT[43] yielding to $\rho^{\pi}_{N1} = 0.06$ and $\rho^{\pi}_{N2} = 0.11$.

3.2.3. Density Functional Calculations of Histidine Model Radicals: Comparison of Hyperfine Data Derived from Density Functional Theory and from EPR Experiments. In previous DFT studies of biological radicals, we have investigated tyrosine,[46] tryptophan,[42] glycine,[47,48] quinones,[37] and the DNA base cytosine.[38] In these studies we have found that an ethyl group is a sufficient and very suitable model for the amino acid or quinone "tail" to the active side group. This is primarily related to the fact that with the ethyl group we are able to obtain a correct description of the two β-protons rather than with a methyl group. As a model for the histidine radical at low pH, studied experimentally in this work, we chose, for the DFT calculations, the 4-ethylimidazole cation radical in which both nitrogens are protonated. Of the various systems, histidine/imidazole is unique in the respect that there are significant data for the nitrogen couplings.

From EPR data, particularly from the occurrence of a large proton coupling of 3.02 mT, an addition of OH radicals to C2, C4, or C5 of the imidazole ring is suggested. The isotropic hfc's, spin densities, and relative energies of these three radicals of the histidine model 4-ethylimidazole have been computed at the PWP86/6-311G(2d,p)//B3LYP/6-31G(d,p) and B3LYP/6-311+G(2df,p)//B3LYP/6-31G(d,p) levels, respectively. The three possible OH adducts were optimized and the hyperfine properties evaluated. The resulting isotropic hfc's and spin densities are shown in Figure 5A−C; they are given in the figure with italic and bold letters, respectively. The energetically lowest lying structure is that where OH attack has occurred on C2, whereas the C5 and C4 adducts lie 10.3 and 14.4 kcal/mol above the one at C2, respectively.

Since advanced DFT approaches, as used here, are able to yield hyperfine coupling constants directly, we compare the isotropic hyperfine coupling constants (hfc's) measured by EPR for the histidine cation radical (see Figure 4) with the hfc's of the protonated 4-ethylimidazole cation radicals calculated by DFT (Figure 5). This procedure is preferred rather than a comparison of theoretical and experimentally determined spin densities, because the Q and Q' factors in the semiempirical formulas for the experimentally estimated π-spin densities, derived from measured isotropic hfc's of α- and β-protons, respectively, are only approximate values and not uniformly valid for different radicals. This is supported also from a comparison of DFT calculations of spin densities with those from experimentally available hfs data for tyrosine radicals.[46]

Imidazole Ring. From the calculated isotropic hfc's for three different species with addition of OH$^{\bullet}$ to C2, C4, or C5, the C4−OH adduct can be ruled out, because of the absence of any large proton coupling constant of about 3.0 mT in the calculation and also because of the near zero spin density at C4. The latter leads to very small β-proton couplings which is in contradiction to the experimental result. The calculated hfc's for the radicals with OH at C2 or C5 both show a large proton hfc (2.67 and 2.71 mT, respectively), but the remaining hfc's of the C5 addition radical fit better to the experimental EPR

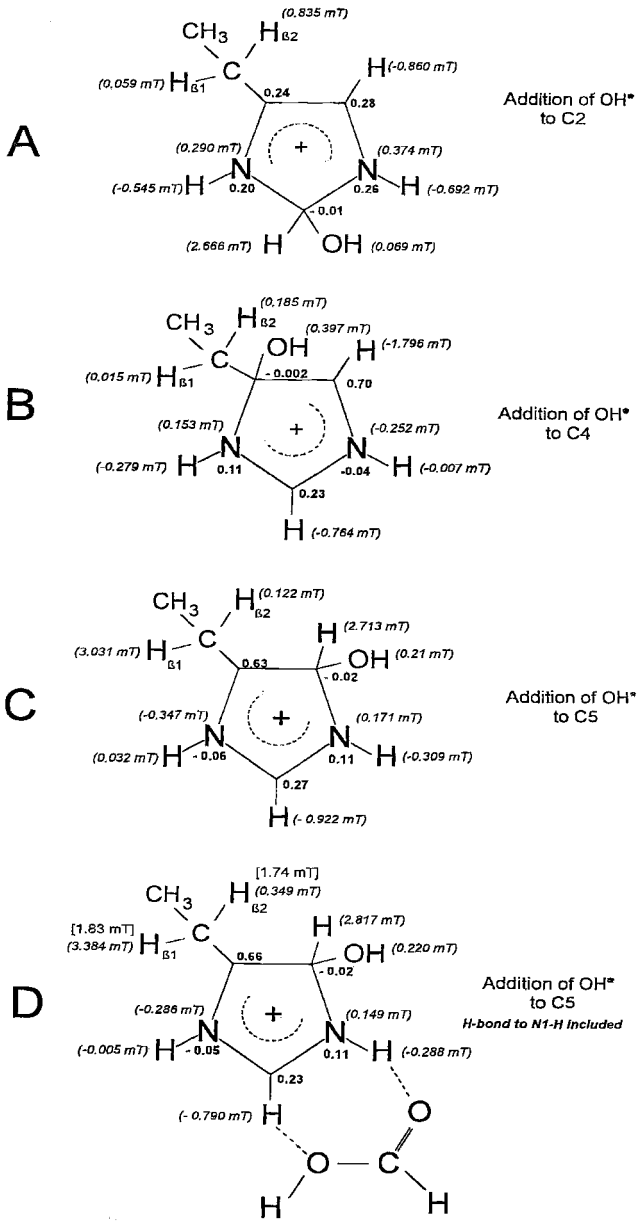

Figure 5. Electronic structure (hyperfine coupling constants and spin densities) *calculated* by DFT of different protonated OH-adduct cation radicals of 4-ethylimidazole, OH additions at the positions C2 (A), C4 (B), and C5 (C) and OH addition at position C5 including a hydrogen-bonded formic acid molecule (D) are shown. Isotropic hyperfine coupling constants (in brackets and italic letters) are given next to the corresponding nuclei; total spin densities are in bold letters. Key: ( ), static values for energy-minimized side chain geometry; Key: [ ], averaged values for side chain motion.

data. The calculated nitrogen hfc's in this radical exhibit the same ratio of 1:2 (and also similar hfc's values) as found by EPR; this is not the case for C2 addition. Furthermore, in the C5-adduct radical the calculated hfc's for the dissociable protons fit better to the experimental one, whereas in case of C2 addition they are larger than the experimental value. Taken together, theoretical data support clearly that the formation of the histidine cation radical at pH 2.0 takes place by addition of OH radicals to the aromatic imidazole ring at the C5 carbon. An oxidation of a ligand histidine has been observed in Cu,Zn superoxide dismutase by HPLC technique upon treatment with H_2O_2.[49] From comparison with 2-oxohistidine the position of attacking the imidazole ring was reported at C2; a comparison with 5-oxohistidine, however, was not included in this study.

There is a good, although not perfect, match with the experimental hfc's of the ring protons and nitrogens for the C5 adduct (Figure 5C), except the C2 α-proton for which the theory predicts a larger value (−0.92 mT) than found in the experiment (−0.59 mT).

Since in aqueous systems the nitrogens of the histidine ring are able to form hydrogen bonds which may influence the spin densities and the hfc's, DFT calculations have been extended to a hydrogen-bonded molecule. In a first attempt to improve the theoretical model, a hydrogen-bonding moiety (formic acid, HCOOH) was added to the C5 adduct, such that the two formic acid oxygens would form hydrogen bonds to the N1 and C2 protons. The system was again fully optimized, and the hyperfine couplings were evaluated. The results shown in Figure 5D demonstrate that the calculated hfc's, particularly those for the two nitrogens, the C2 α-proton, and the C5 proton are significantly closer to the experimental EPR values than those without the formic acid molecule. The nitrogen couplings at N1 and N3 are slightly reduced and are now in better agreement with the experiment. The H(O) and H1 couplings are probably too close to each other to be separable, and each of them may be responsible for the observed 0.21 mT coupling. The value for H2 is decreased to −0.79 mT (experiment: −0.59 mT), and the H5 coupling increases to 2.82 mT (experiment: 3.02 mT); in both cases these are closer to the experimental values.

Considering that an oxidation of the imidazole ring of histidine was reported at the C2 position,[49] a formic acid residue H-bonded to the NH proton and the C2−OH proton for the C2-addition radical (see Figure 5A) was also included in the calculation. The nitrogen hfcc's $a_{N1} = 0.290$ mT and $a_{N3} = 0.374$ mT (without formic acid) and $a_{N1} = 0.358$ mT and $a_{N3} = 0.451$ mT (with formic acid) are even further from the experimental values (0.14 and 0.27 mT) in the case of a H-bonding molecule to the radical with 2-OH addition. The hfc's for NH protons (0.69 and 0.54 mT) in the C2 addition radical remain almost unchanged with H-bonding formic acid and are much larger than the experimental value (0.21 mT). Thus, only the C5 position for histidine oxidation is in accordance with the experimental data. Taking into account the fact that the DFT calculations were performed for a molecule "in vacuum", whereas the experiments were done in aqueous phase at pH 2, the agreement is quite good. The better agreement with the experimental values in the case of additional modelling of the water environment by a H-bond shows that the highly sophisticated DFT approaches are able to describe the actual experimental situation quite well.

As indicated above, the presence of a hydrogen-bonding moiety to the N1/C2 fragment of the molecule, as employed in this work, may well be the reason for the favored C5 radical attack. On the basis of the improved agreement between experimental and computed data, we conclude that at least one hydrogen-bonding group is indeed present in the system.

β-Protons. In order to investigate the dependence of the β-proton hfc's on the orientation relative to the ring plane, the ethyl tail of the C5−OH adduct was rotated about the C4−C_β bond in steps of 10°, at each step reoptimizing the remaining geometric parameters of the ethyl tail. From the resulting energy curve of the variation in the isotropic hfc's of β-protons as a function of the C_α−C_β−C4−N3 rotational angle (not shown), we note that the potential energy for rotation is relatively low, only about 2.5 kcal/mol. In solution at room temperature one may expect that the system undergoes rapid waggling fluctuations about the C4−C_β bond such that the observed β-proton couplings of 1.23 and 1.41 mT are motionally averaged values. A clear indication to rapid rotational motion of the side group is the fact that none of the calculated β-proton hfc's for the energy-minimized *static* conformation are in agreement with the experimentally observed values, irrespective of rotational angle. The calculated *motional average* values for the two β-protons (1.74 and 1.83 mT), however, are not equivalent and are in much closer agreement with the experimental data set. Thus, the computed average data of H_β in the hydrogen-bonded 4-ethyl-5-hydroxyimidazole radical cation, 1.74 and 1.83 mT (see values in brackets in Figure 5D), are regarded as a suitable fit to the experimentally observed couplings. The remaining discrepancy may be due to the smaller model employed; we did not taken into account the full effects of the bulkier amino and carboxylic acid groups of histidine, and all calculations have been performed in vacuum; i.e., we did not include the solvent effects and hydrogen bonds between amino and carboxylic groups of neighboring molecules.

4. Conclusions

Upon oxidation of histidine in a Ti^{3+}/H_2O_2 Fenton system, a histidine−OH adduct cation radical is formed by addition of OH radicals to the C5 carbon of the imidazole ring. The isotropic hyperfine coupling constants of two β-protons, three ring protons, and two nitrogen nuclei of this 5-oxohistidine cation radical have been determined by EPR. This is the first report on a detailed electronic structure—including hyperfine structure of β-protons, protons, and nitrogens of the imidazole ring—of a transient histidine radical in liquid aqueous solution determined by EPR spectroscopy, which is complemented by density functional theory (DFT) calculations. DFT calculations for all hyperfine coupled nuclei and spin densities at ring atoms for three cation radicals of the histidine model 4-ethylimidazole with different positions of OH addition were performed and support the assignment of experimental hfs splittings. Excellent agreement of experimental and theoretical hfs data was achieved for the nuclei of the imidazole ring, particularly when a H-bond to the ring-N1 is included in the calculation of the hfc's (approximating the aqueous environment of the radical).

The question may arise about which are the typical spectral features of histidine radicals. This is important for recognizing them easier in the protein-bound state. As shown in detail for protein-linked tyrosine radicals[2,11] and also for protein-linked tryptophan radicals,[17,18] the conformation of β-methylene protons of protein radicals depends primarily on structural constraints in the immediate protein environment of the radical. This will probably also be valid for protein-linked histidine radicals. A special feature of histidine radicals is the occurrence of two different nitrogen hfc's. In powderlike EPR spectra of protein-linked histidine radicals (in the frozen state and in the immobilized liquid state), however, small and strongly anisotropic nitrogen hfc's as observed in different protein-linked tryptophan radical[17,18] are expected which will usually be resolved only by ENDOR or pulsed EPR (ESEEM) techniques.

The OH-adduct radical of oxidized histidine, however, which exhibits an unusual large proton hf splitting of about 3.0 mT may be recognized easily as an EPR spectroscopic fingerprint. Since a ring proton on a tetragonal-hybridized carbon exhibits properties of β-protons including their small hfs anisotropy,[23] this splitting would certainly be resolved in powderlike EPR spectra of immobilized histidine radicals in proteins.

OH-adduct radicals of histidine as studied here may occur upon oxidative stress when reactive oxygen species are formed in case of a cellular malfunction by reaction of H_2O_2 with free ferrous iron or under conditions of UV photolysis or radiolysis of proteins, in general.

Histidine radicals which may appear transiently during electron transport processes in radical enzymes and metalloproteins will probably keep the imidazole ring intact. To model such histidine radicals in solution, the application of milder oxidants than OH radicals is necessary. Another option to model histidine radicals may be UV irradiation of frozen solution of histidine models, but in this case the EPR spectra are much less resolved[50] and require more sophisticated techniques like ENDOR or pulsed EPR (ESEEM) for hfs analysis.

Acknowledgment. The work was supported by the Deutsche Forschungsgemcinschaft (DFG) Project La 751/2-1, the Fonds der Chemischen Industrie to G.L. and W.L., and the Swedish Natural Science Research Council (NFR). Grants of computer time at the Center for Parallel Computing (PDC) in Stockholm are gratefully acknowledged. We thank Prof. Astrid Gräslund, Department of Biophysics, Stockholm University, for valuable discussion.

References and Notes

(1) Sjöberg, B. M.; Reichard, P.; Gräslund, A.; Ehrenberg, A. *J. Biol. Chem.* **1978**, *253*, 6863.
(2) Gräslund, A.; Sahlin, M. *Annu. Rev. Biophys. Biomol. Struct.* **1996**, *25*, 259.
(3) Dietz, R.; Nastaincyk, W.; Ruf, N. H. *Eur. J. Biochem.* **1988**, *171*, 321.
(4) Berry, B. A. *Photochem. Photobiol.* **1993**, *57*, 179.
(5) Whittaker, M. M.; Whittaker, J. W. *J. Biol. Chem.* **1990**, *265*, 9610.
(6) Kim, S.; Sancar, A.; Essenmacher, C.; Babcock, G. T. *Proc. Natl. Acad. Sci. U.S.A.* **1993**, *90*, 8023.
(7) Huyett, J. E.; Doan, P. E.; Gurbiel, R.; Houseman, A. L. P.; Sivaraja, M.; Goodin, D. B.; Hoffmann, B. M. *J. Am. Chem. Soc.* **1995**, *117*, 9033.
(8) Wagner, A. F. V.; Frey, M.; Neugebauer, F. A.; Schäfer, W.; Knappe, J. *Proc. Natl. Acad. Sci. U.S.A.* **1992**, *89*, 996.
(9) Mulliez, E.; Fontecave, M.; Gaillard, J.; Reichard, P. *J. Biol. Chem.* **1993**, *268*, 2296.
(10) Mao, S. S.; Yu, G. X.; Chalfoun, D.; Stubbe, J. *Biochemistry* **1992**, *31*, 9752.
(11) Sjöberg, B. M. *Nucleic Acids and Molecular Biology*; Eckstein, F., Lilley, D. M. J., Eds.; Springer: Berlin, Heidelberg, 1995; Vol. 9, pp 192−221.
(12) Rao, P. S.; Simic, M.; Hayon, E. *J. Phys. Chem.* **1975**, *79*, 1260.
(13) Boussac, A.; Zimmermann, J. L.; Rutherford, A. W.; Lavergne, J. *Nature* **1990**, *347*, 303.
(14) Zimmermann, J. L.; Boussac, A.; Rutherford, A. W. *Biochemistry* **1993**, *32*, 4831.
(15) Tang, X. S.; Diner, B. A.; Larsen, B. S.; Gilchrist, M.L., Jr.; Lorigan, G. A.; Britt, R. D. *Proc. Natl. Acad. Sci. U.S.A.* **1994**, *91*, 704.
(16) Tang, X. S.; Randall, D. W.; Force, D. E.; Diner, B. A.; Britt, R. D. *J. Am. Chem. Soc.* **1996**, *118*, 7638.
(17) Lendzian, F.; Sahlin, M.; MacMillan, F.; Bittl, R.; Fiege, R; Pötsch, S.; Sjöberg, B.-M.; Gräslund, A.; Lubitz, W.; Lassmann, G. *J. Am. Chem. Soc.* **1996**, *118*, 8111.
(18) Pötsch, S.; Lendzian, F.; Ingemarson, R; Hörnberg, A.; Thelander, L.; Lubitz, W.; Lassmann, G.; Gräslund, A. *J. Biol. Chem.*, submitted for publication.
(19) Brabek, V.; Mornstein, V. *Biophys. Chem.* **1980**, *12*, 159.
(20) Ngo, F. Q.; Budzinski, E. E.; Box, H. C. *J. Chem. Phys.* **1974**, *60*, 3373.
(21) Box, H. C.; Freund, H. G.; Lilga, K. T. *J. Chem. Phys.* **1967**, *46*, 2130.
(22) Westhof, E.; Flossmann, W.; Müller, A. *Int. J. Radiat. Biol.* **1975**, *27*, 51.
(23) Lamotte, B.; Gloux, P. *J. Chem. Phys.* **1973**, *59*, 3365.
(24) Samuni, A.; Neta, P. *J. Phys. Chem.* **1973**, *77*, 1629.
(25) Schmidt, J.; Borg, D. *Radiat. Res.* **1976**, *65*, 220.
(26) Paul, H.; Fischer, H. *Ber. Bunsen-Ges. Phys. Chem.* **1969**, *73*, 972.
(27) Czapski, G. *J. Phys. Chem.* **1971**, *75*, 2957.
(28) Czapski, G.; A. Samuni, A.; Meisel, D. *J. Phys. Chem.* **1971**, *75*, 3271.
(29) Fiege, R. Dissertation, Technical University of Berlin, 1997.
(30) Malkin, V. G.; Malkina, O. L.; Eriksson, L. A.; Salahub, D. R. In *Theoretical and Computational Chemistry, Vol 2, Modern Density Functional Theory-A Tool for Chemistry*; Politzcr, P., Seminario, J. M., Eds.; Elsevier: New York, 1995; pp 273−347.
(31) Barone, V. In *Recent Advances in Density Functional Theory, Part 1*; Chong, D. P., Ed.; World Scientific: Singapore, 1995; pp 287−334. Engels, B.; Eriksson, L. A.; Lunell, S. *Adv. Quantum Chem.* **1996**, *27*, 297.
(32) Slater, J. C. *Quantum Theory of Molecules and Solids*; McGraw-Hill: New York, 1974. Becke, A. D. *Phys. Rev.* **1988**, *A38*, 3098. Vosko, S. H.; Wilk, L.; Nusiar, M. *Can. J. Phys.* **1980**, *58*, 1200. Lee, C.; Yang, W.; Parr, R. G. *Phys. Rev. B* **1988**, *37*, 785. Becke, A. D. *J. Chem. Phys.* **1993**, *98*, 1372.
(33) Perdew, J. P.; Wang, Y. *Phys. Rev. B* **1986**, *33*, 8800. Perdew, J. P. *Phys. Rev. B* **1986**, *33*, 8822. Perdew, J. P. *Phys. Rev.* **1986**, *34*, 7406.
(34) Frisch, M. J.; Trucks, G. W.; Schlegel, H. B.; Gill, P. M. W.; Johnson, B. G.; Robb, M. A.; Cheeseman, J. R.; Keith, T. A.; Peterson, G. A.; Montgomery, J. A.; Raghavachari, K.; Al-Laham, M. A.; Zakrewski, V. G.; Ortiz, J. V.; Foresman, J. B.; Cioslowski, J.; Stefanov, B. B.; Nanayakkara, A.; Challacombe, M.; Pang, C. Y.; Ayala, P. Y.; Chen, W.; Wong, M. W.; Andres, J. L.; Replogle, E. S.; Gomperts, R.; Martin, R. L.; Fox, D. J.; Binkley, J. S.; DeFrees, D. J.; Baker, J.; Stewart, J. P.; Head-Gordon, M.; Gonzalez, C.; Pople, J. A. *Gaussian 94*; Gaussian Inc.: Pittsburgh, PA, 1995.
(35) St-Amant, A.; Salahub, D. R. *Chem. Phys. Lett.* **1990**, *169*, 387. St-Amant, A. Ph.D. Thesis, Univ. de Montreal, 1991. Salahub, D. R.; Fournier, R.; Mlynarski, P.; Papai, I.; St-Amant, A.; Ushio, J. In *Density Functional Methods in Chemistry*; Labanowski, J., Andzelm, J., Eds.; Springer-Verlag: New York, 1993; pp 77−100.
(36) Eriksson, L. A. *Mol. Phys.* **1997**, *91*, 827.
(37) Eriksson, L. A.; Himo, F.; Siegbahn, P. E. M.; Babcock, G. T. *J. Phys. Chem. A* **1997**, *101*, 9496.
(38) Wetmore, S. D.; Himo, F.; Boyd, R. J.; Eriksson, L. A. *J. Phys. Chem. B* **1998**, *102*, 7484.
(39) Fischer, H. *Ber. Bunsen-Ges. Phys. Chem.* **1967**, *71*, 685.
(40) Norman, R. O. C.; West, P. R. *J. Chem. Soc. B (Phys. Org.)* **1969**, 389.
(41) Hellwege, K. H. *Landolt-Börnstein: Numerical Data and Functional Relationships in Science and Technology, Group II, Vol. 9, Magnetic Properties of Free Radicals*; Springer-Verlag: New York, 1979; Part c2, pp 8−25.
(42) Himo, F.; Eriksson, L. A. *J. Phys. Chem. B* **1997**, *101*, 9811.
(43) Wertz, J. G.; Bolton, J. R. *Electron Spin Resonance*; Chapman and Hall: New York, 1986.
(44) Bender, C. J.; Sahlin, M.; Babcock, G. T.; Barry, B. A.; Chandrashekar, T. K.; Salowe, S. P.; Stubbe, J.; Lindström, B.; Peterson, L.; Ehrenberg, A.; Sjöberg, B. M. *J. Am. Chem. Soc.* **1989**, *111*, 8076.
(45) Sealy, R. C.; Harman, L.; West, P. R.; Mason, R. P. *J. Am. Chem. Soc.* **1985**, *107*, 3401.
(46) Himo, F.; Gräslund, A.; Eriksson, L. A. *Biophys. J.* **1997**, *72*, 1556.
(47) Himo, F.; Eriksson, L. A. *J. Chem. Soc., Perkin Trans. 2*, **1997**, 305.
(48) Choi, C. H.; Kertzesz, M.; Karpfen, A. *Chem. Phys. Lett.* **1997**, *276*, 266.
(49) Uchida, K.; Kawakishi, S. *J. Biol. Chem.* **1994**, *269*, 2405.
(50) Berthomieu, C.; Boussac, A. *Biospectroscopy* **1995**, *1*, 187.